Detailed seismic bathymetry beneath Ekstroem Ice Shelf, Antarctica: Implications for glacial history and ice-ocean interaction

Emma C. Smith[1,1,1], Tore Hattermann[2,2,2], Gerhard Kuhn[1,1,1], Christoph Gaedicke[3,3,3], Sophie Berger[1,1,1], Reinhard Drews[4,4,4], Todd A. Ehlers[4,4,4], Dieter Franke[3,3,3], Raphael Gromig[1,1,1], Coen Hofstede[1,1,1], Astrid Lambrecht[5,5,5], Andreas Läufer[3,3,3], Christoph Mayer[6,6,6], Ralf Tiedemann[1,1,1], Frank Wilhelms[1,1,1], and Olaf Eisen[1,1,1]

[1]Alfred-Wegener-Institut Helmholtz-Zentrum für Polar- und Meeresforschung
[2]Norwegian Polar Institute, Tromsø, Norway
[3]Federal Institute for Geosciences and Natural Resources (BGR)
[4]Department of Geosciences, University of Tübingen
[5]Bavarian Academy for Science and Humanities
[6]Bavarian Academy of Sciences and Humanities

November 30, 2022

Abstract

The shape of ice-shelf cavities are a major source of uncertainty in understanding ice-ocean interaction and limit our assessment of the response of the Antarctic ice sheets to climate change. Here we use seismic reflection vibroseis data to map, with unprecedented detail, the bathymetry beneath the Ekström Ice Shelf, Dronning Maud Land. The new bathymetry reveals an inland-sloping trough, reaching depths of 1100 m near the current grounding line, which we attribute to a palaeo-ice stream. The trough does not cross-cut the continental shelf. Conductivity-Temperature-Depth profiles within the ice-shelf cavity reveal the presence of cold water at shallower depths with clear tidal mixing at the ice-shelf margins. It is unknown if warm water is present in the trough, although it has been observed in a similar trough under a neighbouring ice shelf. These similarities suggest this bathymetry is characteristic of Dronning Maud Land ice shelves.

Detailed seismic bathymetry beneath Ekström Ice Shelf, Antarctica: Implications for glacial history and ice-ocean interaction

Emma C. Smith[1], Tore Hattermann[2], Gerhard Kuhn[1], Christoph Gaedicke[3], Sophie Berger[1], Reinhard Drews[4], Todd A. Ehlers[4], Dieter Franke[3], Raphael Gromig[1*], Coen Hofstede[1], Astrid Lambrecht[5], Andreas Läufer[3], Christoph Mayer[5], Ralf Tiedemann[1,6], Frank Wilhelms[1,7], Olaf Eisen[1,6]

[1]Alfred-Wegener-Institut Helmholtz-Zentrum für Polar- und Meeresforschung, Bremerhaven, Germany
[2]Norwegian Polar Institute, Tromsø, Norway
[3]BGR, Federal Institute for Geosciences and Natural Resources, Geozentrum Hannover, Hannover, Germany
[4]Department of Geosciences, University of Tübingen, Tübingen, Germany
[5]Geodesy and Glaciology, Bavarian Academy of Sciences and Humanities, Munich, Germany
[6]Department of Geosciences, University of Bremen, Bremen, Germany
[7]Department of Geosciences, University of Göttingen, Göttingen, Germany

Key Points:

- Vibroseis seismic surveys used to map the ice-shelf cavity beneath Ekström Ice Shelf in Antarctica
- Deep trough with transverse sills and overdeepenings provide evidence of past ice streaming and retreat
- Two ocean circulation regimes inferred in the shallow and deep parts of the cavity

*Now at: University of Cologne, Institute of Geology and Mineralogy, Cologne, Germany

Corresponding author: Emma C. Smith, `emma.smith@awi.de`

Abstract

The shape of ice-shelf cavities are a major source of uncertainty in understanding ice-ocean interactions. This limits assessments of the response of the Antarctic ice sheets to climate change. Here we use vibroseis seismic reflection surveys to map the bathymetry beneath the Ekström Ice Shelf, Dronning Maud Land. The new bathymetry reveals an inland-sloping trough, reaching depths of 1100 m below sea level, near the current grounding line, which we attribute to erosion by palaeo-ice streams. The trough does not cross-cut the outer parts of the continental shelf. Conductivity-temperature-depth profiles within the ice-shelf cavity reveal the presence of cold water at shallower depths and tidal mixing at the ice-shelf margins. It is unknown if warm water can access the trough. The new bathymetry is thought to be representative of many ice shelves in Dronning Maud Land, which together regulate the ice loss from a substantial area of East Antarctica.

Plain Language Summary

Antarctica is surrounded by floating ice shelves, which play a crucial role in regulating the flow of ice from the continent into the oceans. The ice shelves are susceptible to melting from warm ocean waters beneath them. In order to better understand the melting, knowledge of the shape and depth of the ocean cavity beneath ice shelves is crucial. In this study we present new measurements of the sea floor depth beneath Ekström Ice Shelf in East Antarctica. The measurements reveal a much deeper sea floor than previously known. We discuss the implications of this for providing routes for warm ocean waters to melt the base of the ice shelf, and discuss how the observed sea-floor features were formed by historical ice flow regimes. Although Ekström Ice Shelf is relatively small, the geometry described here is thought to be representative of the topography beneath many ice shelves in this region, which together regulate the ice loss from a substantial area of East Antarctica.

1 Introduction

Ice shelves surrounding Antarctica act as buttresses, restraining ice discharge from the continent into the oceans, and therefore regulating Antarctic contributions to sea-level rise (Dupont & Alley, 2005). Mass loss from Antarctica has been accelerating over the past 20 years (IPCC, 2019), driven by increased basal melting of ice shelves (Paolo et al., 2015; Pritchard et al., 2012). Accurate knowledge of the geometry of the ice-shelf cavities and the properties of the water column beneath them are essential for understanding processes active at the ice-shelf ocean interface. Recent studies have highlighted a lack of sub-ice shelf bathymetry as a "major limitation" (Pattyn et al., 2017) for future projections of Antarctic mass balance. Improved bathymetric mapping allows determination of water access pathways and calculation of spatially and temporally variable melt rates (e.g. Cochran et al., 2014; Goldberg et al., 2019; Milillo et al., 2019; Morlighem et al., 2020; Tinto et al., 2019; Pattyn et al., 2017). In addition, sub-ice shelf bathymetry also provides information about ice-dynamic history. Understanding the past ice dynamics and implementing an accurate bathymetry in ice-flow and oceanographic models is a critical step to improve projections of the evolution of the ice sheets.

The coast of Dronning Maud Land (DML), East Antarctica (Fig.1) is fringed by numerous small ice shelves. In this area, satellite-derived melt rates are typically low (Rignot et al., 2013). However, the continental shelf is narrow (Fig.1b), meaning the ice shelves of DML are in close proximity to Warm Deep Water (WDW) masses which flow along the continental slope, making this a potentially sensitive region to future change (Hattermann, 2018; Heywood et al., 2013; Thompson et al., 2018). It has also been highlighted as susceptible to marine ice sheet instability (Morlighem et al., 2020; Ritz et al., 2015). In addition, the ice shelf-ocean interactions along the DML coast play an important role in preconditioning the structure and water-mass properties of the westward flowing boundary current (Fahrbach et al., 1994; Hattermann, 2018). This current is a key control on warm-water inflow toward the Filchner-Ronne Ice Shelf (Hellmer et al., 2017; Timmermann & Hellmer, 2013) and bottom water formation in the Southern Weddell Sea (Meijers et al., 2016; Meredith et al., 2011). The few bathymetric measurements that exist under DML ice shelves have revealed cavities that are much deeper than those included in current gridded data sets of Antarctica (e.g. Fretwell et al., 2013; Morlighem et al., 2020). Under the Fimbul Ice Shelf (Fig.1b), a deep trough within the sub-shelf cavity was discovered (Nøst, 2004) and confirmed to contain modified WDW (Hattermann et al., 2012, 2014). At the front of the Roi Baudouin Ice Shelf, in Eastern DML, an 850 m deep trough is present, which has major consequences when simulating ice-sheet advance and retreat (Berger, 2017; Favier et al., 2016). This emerging picture highlights the need for more accurate bathymetry measurements in this region.

The general lack of bathymetry measurements beneath ice shelves is the result of difficulties in access: radar systems, do not penetrate through the water column; gravity inversions are possible, but without control points are sensitive to assumptions about the underlying geology (Eisermann et al., 2020); drilling through the ice provides limited spatial range and is logistically challenging; and the use of autonomous underwater vehicles is rare, as they require ship support (e.g. Jenkins et al., 2010; Nicholls et al., 2006). Seismic surveys currently provide the most reliable method to map water-column thickness, as well as to image the sea bed below.

Here we address this problem using a specialised vibroseis seismic source and snow streamer system (Eisen et al., 2015) to create a new map of the ice-shelf cavity and seafloor bathymetry beneath the Ekström Ice Shelf, DML. Ekström Ice Shelf (Fig.1) covers an area of approximately 6800 km^2 with basal melt rates of up to 1.1 ma^{-1} (Neckel et al., 2012). It is laterally constrained by the grounded ice rises of Søråsen to the west and Halvfarryggen in the east (Fig. 1c). The present ice-shelf front is less than 20 km from the continental shelf break. Until now, little was known about the bottom topography of the ice-shelf cavity. A number of seismic reflection measurements by Kobarg (1988), suggest a southward deepening of the seafloor with a maximum water-column thickness of 500 m. However, a map of the cavity is currently lacking. We integrate our bathymetric mapping with conductivity-temperature-depth (CTD) data acquired through hot-water drilled access holes in the ice shelf and under sea ice in Atka Bay (Fig. 1c). The combined observations are used to identify the primary implications of this new bathymetry for ice-ocean interaction and ice-dynamic history in the region. They show the urgent need for more measurements of sub-ice-shelf bathymetry along the coast of this sector of Antarctica and for many other ice shelves, where the bathymetry is equally poorly constrained.

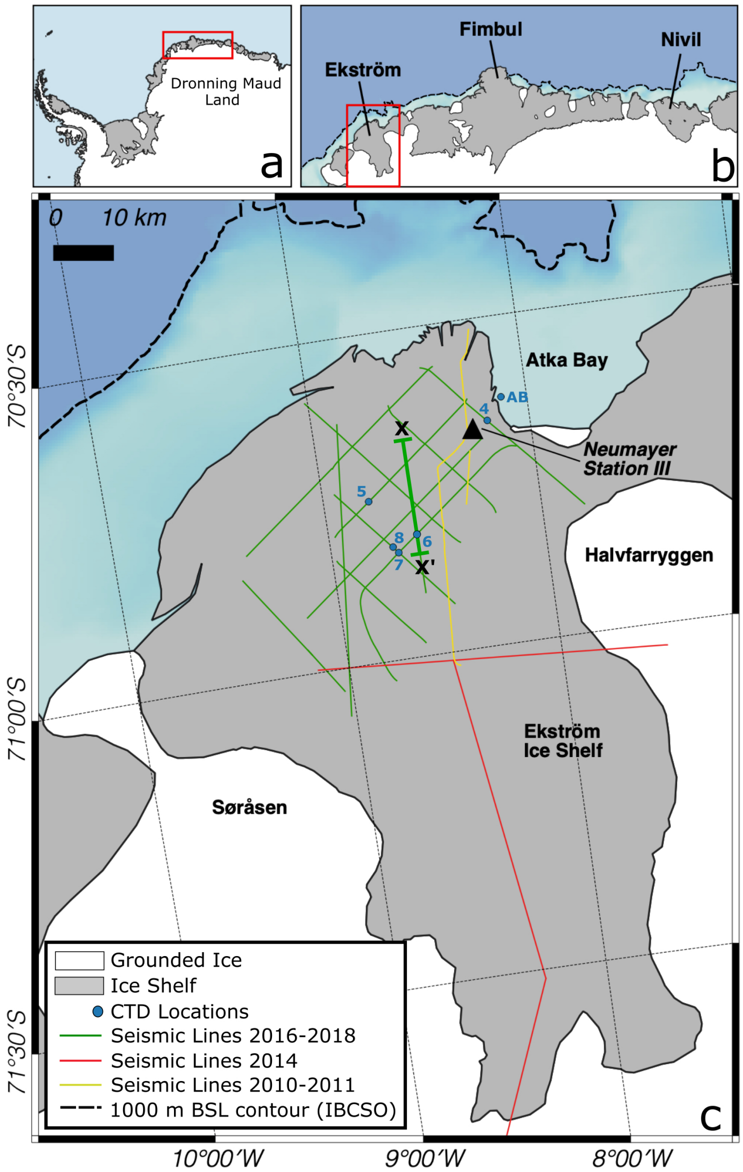

Figure 1. **a)** Location of Dronning Maud Land within Antarctica **b)** Area highlighted in (a) with location of Ekström Ice Shelf indicated and **c)** Ekström Ice Shelf with seismic survey lines and CTD locations shown. In all figures the ice shelf is shown in grey and grounded ice in white. In (b) and (c) the ocean background is from the International Bathymetric Chart of the Southern Ocean (IBCSO) (J. E. Arndt et al., 2013), with the 1000 m below sea level (BSL) contour shown as a dashed line, indicating the location of the continental slope. The CTD location labels, ‘4’ to ‘8’ refer to hot-water drilled access holes ‘EIS-4’ to ‘EIS-8’, and ‘AB’ to the location of a sea-ice lead in Atka Bay. The location of the seismic line shown in Fig. 2 is X-X’.

2 Data and Methods

2.1 Seismic Data Acquisition

Seismic data were collected between 2010 and 2018, using two different vibroseis seismic sources. The snow streamer, used for all data acquisition, was 1500 m long, containing 60 channels, with a 25 m group spacing. Each group contained eight gimballed P-wave SM-4, 14 Hz geophones. For all data collection the vibroseis source was towed behind a snow tractor with the snow streamer towed behind that. This method of operation allowed for data acquisition rates of up to 20 km per day for 10 fold data. Fold refers to the amount of times a sub-surface point (referred to as a common mid-point or CMP) is sampled by different source/receiver pairs. A more detailed explanation of both these seismic sources, the snow streamer, and the operational method is given in Eisen et al. (2015).

The main grid of data, at the ice shelf front, was collected during the 2016/17 and 2017/18 austral summers (Fig.1c, green) as part of the Sub-EIS-Obs project (Kuhn & Gaedicke, 2015). The seismic source was the AWI IVI EnviroVibe, producing a 10 second linear sweep from 10-220 Hz. These data are relatively high fold (6-15), with the exception of the two lines in the north-western corner of the grid, which are single fold. It was not possible to extend data collection further west due to surface crevassing. The seismic lines extending across the grounding line to the east and south were collected in 2014 (Fig.1c, red), using the same acquisition configuration, and are single fold. Three older lines from 2010 and 2011 overlap the main grid (Fig.1c, yellow) and were acquired using the University of Bergen Failing Y-1100 vibroseis source (Kristoffersen et al., 2014), with a 10 second sweep from 10-100 Hz; fold varies between 1 and 8.

All seismic data were processed specifically for this study, to ensure consistent treatment of data from different surveys (supporting information S1). The resulting seismic time-stacked sections all have clear ice base and the sea floor reflections (Fig. 2). The two-way traveltimes (TWTs) of these reflections were hand-picked on each section.

2.2 Depth Conversion and Gridding of Seismic Measurements

The hand-picked TWTs from all seismic lines were used to create grids of the TWT to the ice base and sea floor, using a kriging algorithm. Any mis-ties between picks, in

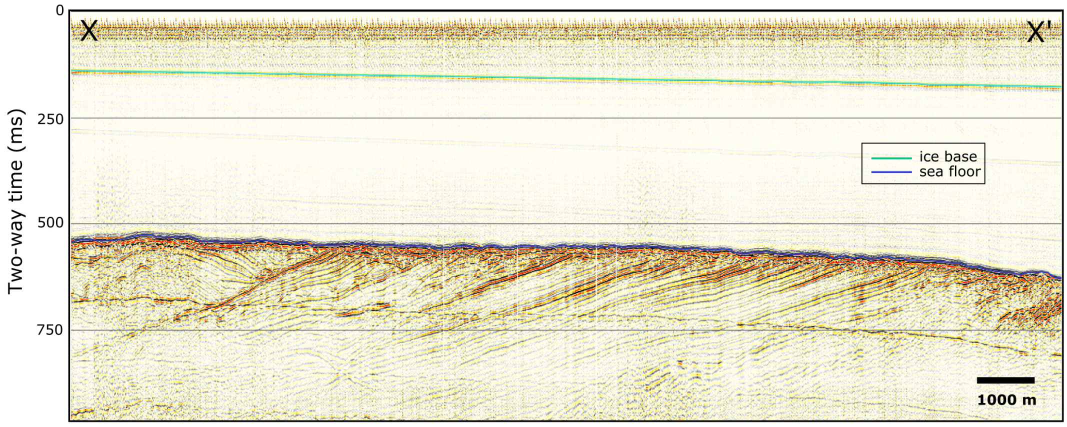

Figure 2. Example of a seismic time-stacked section. Location of section is marked X-X' on Fig. 1, AWI line number 20170561. Reflections from the ice-shelf base and sea floor are clearly visible, and the TWT to them can be easily determined. The section is vertically exaggerated by a factor of 10.

areas where seismic lines overlap, were handled by assigning priority to the higher resolution surveys. Each grid was then depth converted using a seismic velocity of 3601 ms^{-1} for the ice shelf and 1451 ms^{-1} for the water column (supporting information S2). The final step was to correct the depth of each grid for the ice surface elevation, using the REMA digital elevation model v1.1 (Howat et al., 2019), which was re-referenced to the GL04C geoid (Förste et al., 2008).

2.3 Uncertainties in Seismic Depths

Uncertainties in the sea-floor depth, from seismic measurements, come from four main sources: (i) accuracy of the horizon picking, (ii) velocities used for depth conversion of these horizons, (iii) errors in the REMA DEM used for surface elevation corrections and (iv) depth errors from unmigrated data. A detailed analysis of these individual error sources was made (supporting information S3), resulting in cumulative error at the sea floor of ± 14.8 m in the area of the main data grid and ± 34.4 m in the areas of the 2014 seismic lines, which extend from the main grid towards the grounding lines (Fig. 1). The gridded bathymetry may have larger errors away from the seismic lines.

It was possible to measure the ice thickness and sea-floor depth at the five hot-water drilled access hole locations (4-8; Fig. 1) on the ice shelf, both during drilling and with camera equipment and coring devices deployed through the holes to the sea floor. These measurements confirmed that the seismic determined ice thickness was within $\pm$ 5 m of the measured thickness and the sea floor within $\pm$ 10-20 m. This validates our error estimates, as the latter range also includes horizontal displacement of the sampling rope by ocean currents.

2.4 CTD Data

During the 2018/19 austral summer, hot-water drilled access holes were made at five locations on the ice shelf (4-8; Fig. 1). An RBR Concerto CTD sensor was repeatedly lowered through each hole and additionally through a sea-ice lead in Atka Bay (AB; Fig. 1), giving a total of 6 CTD measurement sites. The CTD sensor recorded water mass properties at a frequency of 1 Hz (vertical resolution of 0.5 - 2 m), from which pressure, in-situ temperature, and practical salinity data were extracted (see supporting information S4). The uncertainty for in-situ temperature is 0.02°C and for practical salinity 0.03. These data were used to calculate seismic velocities for depth conversion of the sea-floor seismic reflection (supporting information S2), and to investigate water masses present beneath the ice shelf and sea ice.

3 Results and Discussion

The new sub-ice shelf bathymetry (Fig. 3a) is independent of any previously available products of ice thickness and water depth. Here, we compare the new bathymetry to the Bedmap2 (Fretwell et al., 2013) Antarctic bed topography (Fig. 3b), which has been the baseline Antarctic dataset for the large majority of modelling studies. We highlight the differences to emphasise the need for dedicated measurements of sub-ice shelf bathymetry.

Given the lack of previously available data, the Bedmap2 (Fretwell et al., 2013) seafloor bathymetry beneath Ekström Ice Shelf closely follows the ice-base topography, deepening towards the grounding line. This suggesting a relatively thin, uniform water-column height of the ice shelf cavity (Fig. 3b). The new seismic bathymetry, in contrast, reveals a much more distinct geometry of the ice shelf cavity (Fig. 3c). Similar mismatches have been documented for other ice shelves in this sector (e.g. Nøst, 2004).

Beneath the main grid of our data (Fig. 3a) we find a bathymetric trough under the central part of the ice shelf, which appears to be aligned with the current ice-flow direction. In this area the trough is 30 km wide and reaches depths of up to 800 m below sea level (Figs. 3a and 3c, C-C'). The trough flanks have depths around 450-500 m (Figs. 3a and 3c, C-C' and D-D'), shallowing to around 300 m depth at the marginal grounding line joining the ice shelf to the ice rise of Halvfarryggen (Figs. 3a and 3c, B-B'). Shallowing topography is also seen towards the western grounding line at Søråsen and it is likely this mirrors the cavity shape to the east. The sea floor directly in front of the ice shelf is 450 m deep, similar to the flanks of the trough. A basin-like depression, around 570 m deep, is seen on the eastern plateau, to the south of Neumayer Station III. The profile from the front of the ice-shelf edge to the current grounding line (Figs. 3a and 3c, A-A'), follows the axis of the trough under the main grid and the single seismic line connecting the south of the grid to the grounding line. This indicates an inland-sloping sea floor (Figs. 3a and 3c, A-A'), reaching a maximum depth of 1100 m around 10 km seaward of the current grounding line.

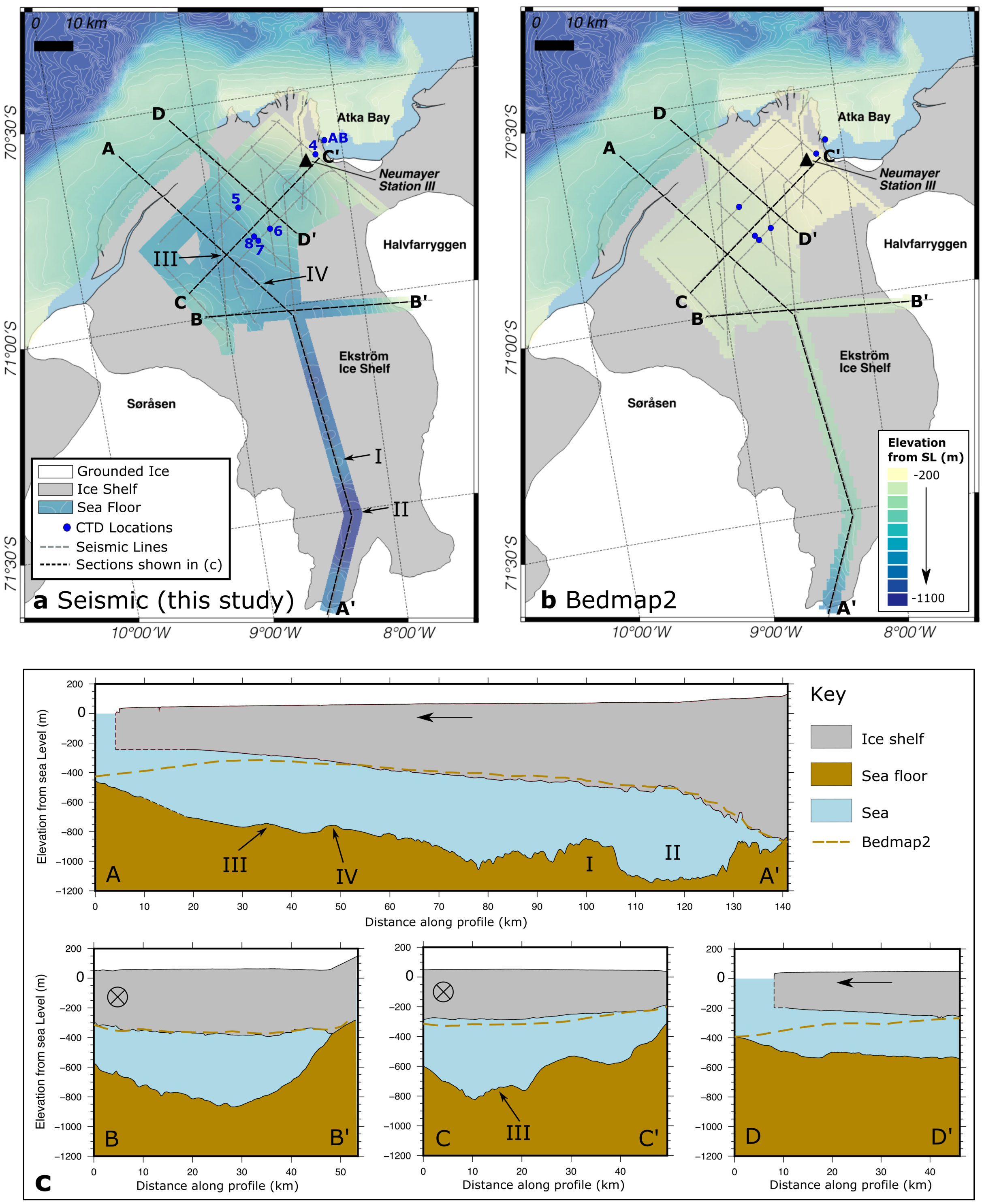

Figure 3. Caption on next page

Figure 3. a) Gridded sea-floor bathymetry beneath the Ekström Ice Shelf, derived from seismic measurements (this study). **b)** The same area as (a) but with sub-ice shelf bathymetry from Bedmap2 (Fretwell et al., 2013) co-located with the seismic bathymetry. In both (a) and (b) bathymetry seawards of the ice-shelf edge is from the IBCSO (J. E. Arndt et al., 2013) mapping project and is cut to the area where measurements are present, note that ice shelf front was further landward than present day when some measurements were made. White contours are at 50 m intervals. Features I-IV are indicated (see text for details). Grey dashed lines show the seismic data locations, with the cross sections shown in (c) indicated by black dashed lines. Blue points indicate the location of CTD measurements, as in Fig. 1.**c)** Cross sections of the ice-shelf cavity and sea floor beneath and in front of Ekström Ice Shelf. Ice flow direction is indicated by arrows and cross-hairs. Sea-floor bathymetry (brown) is from the seismic grid merged with IBSCO, seaward of the ice-shelf edge. The ice shelf (grey) is derived from gridded seismic data at the ice base and REMA surface elevation. Solid black outlines are areas where data is present, dashed lines in A-A' and D-D' are data gaps. Bedmap2 elevations are shown as brown dashed lines for comparison. All data are referenced to the GL04C geoid.

3.1 Ice-Dynamic History

The sea-floor bathymetry under Ekström Ice Shelf allows us to interpret features associated with past ice sheet configurations in this region. The deepened trough under the centre of the ice shelf (Fig. 3a) is interpreted as a relict landscape, formed through erosion by former ice streams. The flanks of the trough and the sea floor at the ice-shelf front are around 300-400 m shallower than the trough. The trough does not cross-cut the outer parts of continental shelf and it is therefore likely that the seaward rising continental shelf was a previous grounding line.

Sediment core records in front of Ekström Ice Shelf are sparse (Grobe & Mackensen, 1992; Hillenbrand et al., 2014) and do not provide conclusive evidence as to whether grounded ice covered the entire continental shelf, as far as the continental slope (approximately the 1000 m contour in Fig. 1), during the Last Glacial Maximum (LGM: 23 - 19 ka BP). Sediment cores from the continental shelf, in front of Ekström Ice Shelf, were not deep enough to penetrate into material from the LGM. The recovered Holocene aged sediments (11.7 ka BP to present), were likely deposited beneath an ice shelf (Grobe & Mackensen, 1992), close to the grounding line. Our finding that the trough does not cross-cut the outer parts of continental shelf suggests that grounded ice likely reached to the inner parts of the continental shelf (around the current ice-shelf front) in the past, possibly at the LGM, but the precise grounding line position remains unresolved.

The seismic line extending from the main grid to the south (Fig. 3c, A-A') shows a sea floor that deepens towards the current grounding line. The general trend of a retrograde slope within the trough would likely have put this area at risk of rapid ice retreat after the LGM, until a stable grounding line position (e.g a topographic high) was reached. There are a number of topographic highs along the ice-flow direction. Particularly prominent is the topographic high at 100 km along profile A-A' (I; Fig. 3c), which is around 200 m above the surrounding sea floor. We suggest that this is a former grounding line position, given its significant elevation. However, current bathymetry measurements in this region do not extend laterally to confirm the extent of this feature. There is a significant overdeepening upstream of this high (II; Fig. 3c), reaching 1100 m depth around 10 km seaward of the current grounding line. Overdeepenings are commonly formed in areas of convergent ice stream flow, where ice velocities and erosional potential are high (Patton et al., 2016). The location of this overdeepening is at the convergence of two tributary glaciers, with higher modern-day ice flow velocities than the surrounding ice (Neckel et al., 2012). When ice was thicker and grounded further seaward, the overdeepened area would have been at the junction between these two tributaries, eroding the deep basin. Overdeepenings typically terminate in sills (Benn & Evans, 2014), where ice flow becomes less constrained, which could explain the origin of the topographic high we observe at 100 km along profile A-A'. Two smaller topographic highs at 35 km (III; Fig. 3c) and 45 km (IV; Fig. 3c) along profile A-A' are around 50 m in height, each separated by deeper basin areas, indicative of ice having been grounded at these points for some time.

A deep central trough punctuated with transverse topographic highs has also been observed under the neighbouring Fimbul Ice Shelf (Nøst, 2004) and along the adjacent Coats Land ice margin (Hodgson et al., 2018, 2019). Under the front of Roi Baudouin Ice Shelf, Eastern DML, an 850 m deep trough (Berger, 2017; Favier et al., 2016) is present, hinting that this may also extend under the ice shelf in a similar way. This emerging picture suggests such deep troughs are ubiquitous in this sector of East Antarctica, indicating ice-streams were a prevalent feature in the past and supporting the need for more widespread sub-ice shelf bathymetry measurements.

3.2 Ice-Ocean Interaction

The implications for ice-ocean interactions in the Ekström region, from the newly mapped ice shelf cavity, refine our understanding of the role of DML ice shelves for the Antarctic ice-sheet mass balance. Along this sector of the Antarctic coast, WDW masses are suppressed below the continental shelf break (Heywood et al., 2013) by the prevailing easterly winds in the 'fresh shelf' regime (Thompson et al., 2018) that extends from about 20 W to 30 E. The sub-ice shelf CTD profiles (Fig. 4) confirm this, underpinning the relatively low basal melt rate estimates (Neckel et al., 2012) for the Ekström Ice Shelf. Most of the cavity is filled with relatively cold Eastern Shelf Water (ESW) that resides above the WDW along the DML coast (Nøst et al., 2011). In-situ temperatures are close to the surface freezing point around -1.9 °C and practical salinity around 34.4. Only the upper tens of meters of the individual profiles show colder (Fig. 4a), less saline water masses, indicating buoyant outflows of Ice Shelf Water (ISW) in a surface layer near the ice shelf base, that is aligned along common melt water mixing line (Fig. 4b, Gade (1979)) originating from the ESW.

Although the deeper trough beneath the central part of the ice shelf does not cross-cut the continental shelf break, it provides a possible conduit for warmer inflows reaching onto the continental shelf to enter the ice shelf cavity (Fig. 3c, A-A'). Intermittent, warmer near-bottom inflows have been observed across a slightly deeper sill beneath the neighbouring Fimbul Ice Shelf (Hattermann et al., 2012) and a rise of WDW along the DML coast has been suggested as a possible response to future climate change (Hattermann, 2018; Hellmer et al., 2017). In these scenarios, the newly revealed several hundred meters of water depth of the Ekström cavity would support a cavity overturning circulation, where warm near-bottom inflows can propagate undiluted toward the grounding line, rendering Ekström Ice Shelf more vulnerable to warm inflows than implied by previous bathymetric datasets. Our example is also likely to be instructive for many smaller, unmapped ice shelves that have a similar configuration and glacial history along the DML coast and elsewhere.

The presence of extensive ocean cavities beneath Ekström and potentially other DML ice shelves has implications for the susceptibility to local marine ice sheet instability (Morlighem et al., 2020; Ritz et al., 2015), as well as for far field effects through melt induced altering water-mass properties of the westward boundary current. While ice-shelf melt water presently contributes little to the freshening of the ESW (Zhou et al., 2014), there is growing evidence that basal melting feedbacks play an important role for the slope front overturning that controls the depth of the thermocline at the shelf break (e.g. Hattermann, 2018). This regulates the access of warm water to the vast Filchner-Ronne Ice Shelf in the Southern Weddell Sea (e.g. Hellmer et al., 2017). A correct representation of the warm water pathways to the ice shelves upstream of the Filchner Trough will hence be crucial to quantifying these effects and assessing the uncertainty of model projections.

Locally, our observed seafloor bathymetry suggests a separation of different circulation regimes beneath the ice shelf. While the central part of the cavity seems to be dominated by the trough system; the eastern portion of the ice shelf, adjacent to Atka Bay, comprises a relatively shallow water column (Figs. 3a and 3c, C-C') that is likely subject to intense tidal mixing and may be responsible for the vigorous accretion of marine ice in the area (S. Arndt et al., 2020). The two successive temperature profiles from the EIS-4 site confirm the existence of a tidally mixed zone in this region. While the EIS-4b profile shows a similar vertical gradient in temperature to the profiles obtained in the deeper part of the cavity, the EIS-4i profile has a more homogeneous vertical temperature structure. The EIS-4i profile was taken about 11 hours later than EIS-4b and according to the CATS regional tidal model (Padman et al., 2008), a relatively large amplitude tidal wave passed the EIS-4 hole location between the two measurements. Hoppmann et al. (2015) found that platelet ice crystals leave the ice shelf cavity in intermittent pulses at this location, and similar tidal flushing events may be responsible for mixing larger volumes of potentially super-cooled ISW in shallower depths, contributing to the platelet ice formation under the fast ice in Atka Bay that has been identified as a prominent habitat in the sea-ice ecosystem (e.g. Smetacek et al., 1992). A recent study also shows that propagating tidal waves may play an important role in modulating basal melting near the ice shelf grounding lines (Sun et al., 2019), further emphasising the need for knowledge of the local cavity shape to assess and interpret the melt rate variability of a given region.

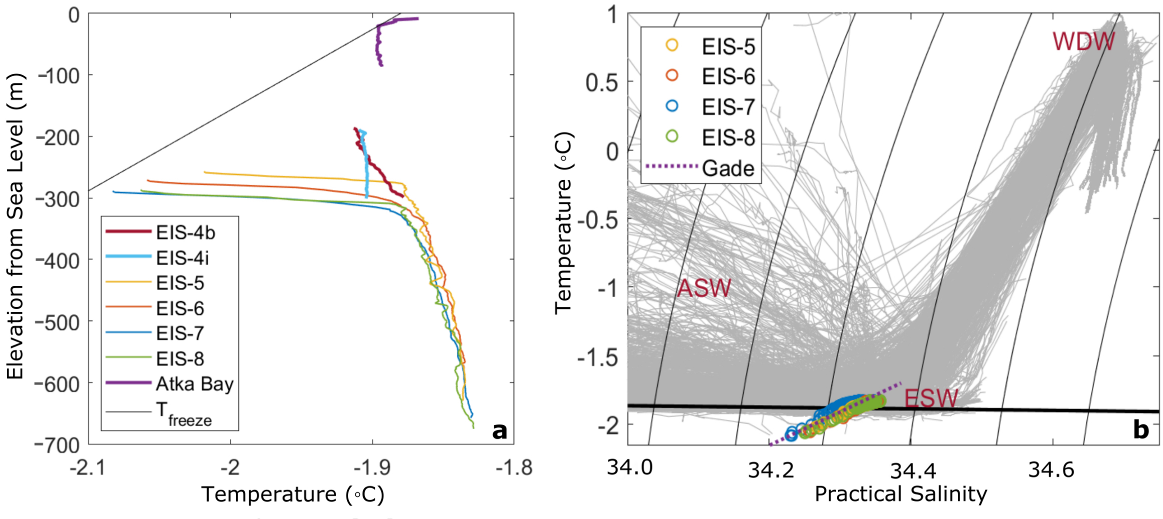

Figure 4. Vertical CTD profiles taken through hot-water drilled access holes (4-8; Fig. 3a) and a sea-ice lead (AB; Fig. 3a) **a)** In-situ temperature observed at different sites beneath Ekström Ice Shelf, and beneath sea ice in Atka Bay. Black line indicates the pressure-dependent melting point temperature for a given practical salinity of 34.25. **b)** Distribution of in-situ temperature and practical salinity profiles at the sites where reliable salinity measurements could be obtained. Gray profiles show the regional subset of open ocean CTD profiles presented in Hattermann (2018), indicating ambient water masses with abbreviations indicating the end members of Warm Deep Water (WDW), Eastern Shelf Water (ESW) and Antarctic Surface Water (ASW). The dashed purple line is the melt water mixing line along which a given water mass may transform through interaction with the ice shelf (Gade, 1979) when assuming zero conductive heat flux into the ice. Black curves indicate horizons of constant density, the thick near-horizontal black line indicates the melting point temperature at atmospheric pressure.

4 Conclusions

We have presented new bathymetry data from under the Ekström Ice Shelf, Dronning Maud Land, Antarctica. The use of vibroseis seismic reflection surveys proves an effective method for collecting high resolution data across large areas of the ice shelf. As a result, the Ekström Ice Shelf cavity is currently one of the best mapped in Antarctica. The discovery of a deep trough with transverse sills under Ekström Ice Shelf is the second example of such a feature under a DML ice shelf, after the neighbouring Fimbul Ice Shelf, with similar features also found along the adjacent Coats Land margin (Hodgson et al., 2018, 2019) and at the ice-shelf front of Roi Baudouin (Berger, 2017; Favier et al., 2016) . This growing list of evidence suggests that the bathymetry we see at Ekström, Fimbul and along the Coats Land coast is likely characteristic of other ice shelves in the DML and neighbouring regions. While these ice shelves are small, they are numerous and very little is known about the cavity geometry, which is a fundamental gap in our ability to understand past ice dynamics and future stability of this region. The ice shelves of DML are known to play a key role in preconditioning the water-mass properties of the westward flowing boundary current, which affects the much larger Filchner-Ronne Ice Shelf and thus large portions of the West Antarctica Ice Sheet. Improved knowledge of ice-shelf cavities is a key required step towards better understanding and projections of the fate of marine ice sheets in a warming climate.

Acknowledgments

Field work and data processing by ECS since 2016 was funded through the AWI-BGR Sub-EIS-Obs Project. ECS was additionally funded through the DFG Cost S2S project, grant number EI672/10-1 in the framework of the priority programme “Antarctic Research with comparative investigations in Arctic ice areas”, RD by the grant MA 3347/10-1, EH 329/13-1 and DR 822/3-1. The field work of A. Lambrecht in 2010 was kindly supported by the Institute of Meteorology and Geophysics, University of Innsbruck, Austria. SB was partly funded by the MIMO (Monitoring melt where Ice Meets Ocean) project, Belgian Science Policy contract No. SR/00/336. We thank R. Blenkner, J. Köhler, H. Schubert, J. Tell, B. Ehlers, S. Hilmarsson and the staff at Neumayer Station III for logistical and other support. N. Koglin for discussion on hot-water drilled access hole locations and geological constraints. The authors would like to thank C. Haas and J-L. Tison for loan on the CTD equipment, D. Hodgson and one anonymous reviewer for constructive and detailed feedback and Emerson E&P Software, Emerson Automation Solutions, for providing licenses for the seismic software Paradigm, in the scope of the Emerson Academic Program. The initial idea for envisaging a geologic drilling underneath Ekström Ice Shelf was put forward by Y. Kristoffersen, who's stimulating creativity and technical support over the years the authors would like to acknowledge in particular. The gridded bathymetry data and CTD data are archived with PANGAEA (https://www.pangaea.de/), the doi for each data set will be provided on acceptance of the paper.

Author Contributions: All authors contributed to seismic target and profiling design, discussed the manuscript and contributed comments towards the final version. ECS designed and wrote the paper, performed fieldwork and led one field season, analysed and interpreted seismic data; TH analysed CTD data and provided the oceanographic component to the paper; DF and A Lambrecht performed seismic data acquisition and analysis, CM performed seismic data acquisition and led one field season, SB acquired and analysed CTD data and provided glaciological constrains for ice shelf processes, RD, TAE and CM contributed ice-flow modelling results and glaciological/geological constraints for data interpretation, CH was in charge of the seismic equipment and processed seismic data, GK, CG, A Läufer and RT provided geological constraints for data interpretation, FW prepared and coordinated the hot water drilling system, RG led one field season and performed cavity sampling, OE coordinated and implemented the seismic field work, led three field seasons, performed seismic and CTD data acquisition. GK, CG, A Läufer, RT, FW and OE are project Co-PIs, designed financial support and project implementation, CG and OE administratively coordinated the project. The trans-disciplinary science component is based on Kuhn and Gaedicke (2015).

References

Arndt, J. E., Schenke, H. W., Jakobsson, M., Nitsche, F. O., Buys, G., Goleby, B., ... Wigley, R. (2013). The International Bathymetric Chart of the Southern Ocean (IBCSO) Version 1.0-A new bathymetric compilation covering circum-Antarctic waters. *Geophysical Research Letters*, *40*(12), 3111–3117. doi: 10.1002/grl.50413

Arndt, S., Hoppmann, M., Schmithüsen, H., Fraser, A. D., & Nicolaus, M. (2020). Seasonal and interannual variability of landfast sea ice in Atka Bay, Weddell Sea, Antarctica. *The Cryosphere Discussions*(January), 1–26. doi:

http://doi.org/10.5194/tc-2019-293

Benn, D., & Evans, D. J. A. (2014). Erosional Processes, Forms and Landscapes. In *Glaciers and glaciation* (2nd ed., p. 816). Routlage.

Berger, S. (2017). *Stability of Antarctic ice shelves - A case study of Roi Baudoin Ice Shelf, Dronning Maud Land, East Antarctica* (PhD). Université Libre De Bruxelles.

Cochran, J. R., Jacobs, S. S., Tinto, K. J., & Bell, R. E. (2014). Bathymetric and oceanic controls on Abbot Ice Shelf thickness and stability. *The Cryosphere*, *8*(3), 877–889. doi: 10.5194/tc-8-877-2014

Dupont, T. K., & Alley, R. B. (2005). Assessment of the importance of ice-shelf buttressing to ice-sheet flow. *Geophysical Research Letters*, *32*(4), n/a–n/a. doi: 10.1029/2004GL022024

Eisen, O., Hofstede, C., Diez, A., Kristoffersen, Y., Lambrecht, A., Mayer, C., ... Hilmarsson, S. (2015). On-ice vibroseis and snowstreamer systems for geoscientific research. *Polar Science*, *9*(1), 51–65. doi: 10.1016/j.polar.2014.10.003

Eisermann, H., Eagles, G., Ruppel, A., Smith, E. C., Jokat, W., & Resources, N. (2020). Bathymetry beneath ice shelves of western Dronning Maud Land , East Antarctica , and implications on ice shelf stability. *Geophysical Research Letters (in review).*

Fahrbach, E., Rohardt, G., Schröder, M., & Strass, V. (1994). Transport and structure of the weddell gyre. *Annales Geophysicae*, *12*(9), 840–855. doi: 10.1007/s00585-994-0840-7

Favier, L., Pattyn, F., Berger, S., & Drews, R. (2016). Dynamic influence of pinning points on marine ice-sheet stability: A numerical study in Dronning Maud Land, East Antarctica. *The Cryosphere*, *10*(6), 2623–2635. doi: 10.5194/tc-10-2623-2016

Förste, C., Schmidt, R., Stubenvoll, R., Flechtner, F., Meyer, U., König, R., ... Esselborn, S. (2008). The GeoForschungsZentrum Potsdam/Groupe de Recherche de Gèodésie Spatiale satellite-only and combined gravity field models: EIGEN-GL04S1 and EIGEN-GL04C. *Journal of Geodesy*, *82*(6), 331–346. doi: 10.1007/s00190-007-0183-8

Fretwell, P., Pritchard, H. D., Vaughan, D. G., Bamber, J. L., Barrand, N. E., Bell, R., ... Zirizzotti, A. (2013). Bedmap2: improved ice bed, surface and thickness datasets for Antarctica. *The Cryosphere*, *7*(1), 375–393. doi: 10.5194/tc-7-375-2013

Gade, H. G. (1979). Melting of Ice in Sea Water: A Primitive Model with Application to the Antarctic Ice Shelf and Icebergs. *Journal of Physical Oceanography*, *9*(1), 189–198. doi: 10.1175/1520-0485(1979)009⟨0189:MOIISW⟩2.0.CO;2

Goldberg, D. N., Gourmelen, N., Kimura, S., Millan, R., & Snow, K. (2019). How Accurately Should We Model Ice Shelf Melt Rates? *Geophysical Research Letters*, *46*(1), 189–199. doi: 10.1029/2018GL080383

Grobe, H., & Mackensen, A. (1992). Late Quaternary climatic cycles as recorded in sediments from the Antarctic continental margin. In *Antarctic research series* (Vol. 56, pp. 349–376). doi: 10.1029/AR056p0349

Hattermann, T. (2018). Antarctic Thermocline Dynamics along a Narrow Shelf with Easterly Winds. *Journal of Physical Oceanography*, *48*(10), 2419–2443. doi: 10.1175/JPO-D-18-0064.1

Hattermann, T., Nøst, O. A., Lilly, J. M., & Smedsrud, L. H. (2012). Two years of oceanic observations below the Fimbul Ice Shelf, Antarctica. *Geophysical Research Letters*, *39*(12), n/a–n/a. doi: 10.1029/2012GL051012

Hattermann, T., Smedsrud, L. H., Nøst, O. A., Lilly, J. M., & Galton-Fenzi, B. K. (2014). Eddy-resolving simulations of the Fimbul Ice Shelf cavity circulation: Basal melting and exchange with open ocean. *Ocean Modelling*, *82*, 28–44. doi: 10.1016/j.ocemod.2014.07.004

Hellmer, H. H., Kauker, F., Timmermann, R., & Hattermann, T. (2017). The Fate of the Southern Weddell Sea Continental Shelf in a Warming Climate. *Journal of Climate*, *30*(12), 4337–4350. doi: 10.1175/JCLI-D-16-0420.1

Heywood, K. J., Locarnini, R. A., Frew, R. D., Dennis, P. F., & King, B. A. (2013, mar). Transport and Water Masses of the Antarctic Slope Front System in The Eastern Weddell Sea. In *Antarctic research series* (Vol. 75, pp. 203–214). Retrieved from `http://doi.wiley.com/10.1029/AR075p0203` doi: 10.1029/AR075p0203

Hillenbrand, C.-d., Bentley, M. J., Stolldorf, T. D., Hein, A. S., Kuhn, G., Graham, A. G., … Sugden, D. E. (2014). Reconstruction of changes in the Weddell Sea sector of the Antarctic Ice Sheet since the Last Glacial Maximum. *Quaternary Science Reviews*, *100*, 111–136. doi: 10.1016/j.quascirev.2013.07.020

Hodgson, D. A., Hogan, K., Smith, J. M., Smith, J. A., Hillenbrand, C. D., Graham, A. G., … Larter, R. (2018). Deglaciation and future stability of the Coats Land ice margin, Antarctica. *The Cryosphere*, *12*(7), 2383–2399. doi: 10.5194/tc-12-2383-2018

Hodgson, D. A., Jordan, T. A., De Rydt, J., Fretwell, P. T., Seddon, S. A., Becker, D., … Vaughan, D. G. (2019). Past and future dynamics of the Brunt Ice Shelf from seabed bathymetry and ice shelf geometry. *The Cryosphere*, *13*(2), 545–556. doi: 10.5194/tc-13-545-2019

Hoppmann, M., Nicolaus, M., Paul, S., Hunkeler, P. A., Heinemann, G., Willmes, S., … Gerdes, R. (2015). Ice platelets below Weddell Sea landfast sea ice. *Annals of Glaciology*, *56*(69), 175–190. doi: 10.3189/2015AoG69A678

Howat, I. M., Porter, C., Smith, B. E., Noh, M.-J., & Morin, P. (2019). The Reference Elevation Model of Antarctica. *The Cryosphere*, *13*(2), 665–674. doi: 10.5194/tc-13-665-2019

IPCC. (2019). *IPCC Special Report on the Ocean and Cryosphere in a Changing Climate [H.-O. Pörtner, Roberts, D. C., Masson-Delmotte, V., Zhai, P., Tignor, M., Poloczanska, E., Mintenbeck, K., Nicolai, M., Okem, A., Petzold, J. Rama, B. Weyer, N. (eds.)]* (Tech. Rep.). doi: https://www.ipcc.ch/report/srocc/

Jenkins, A., Dutrieux, P., Jacobs, S. S., McPhail, S. D., Perrett, J. R., Webb, A. T., & White, D. (2010). Observations beneath Pine Island Glacier in West Antarctica and implications for its retreat. *Nature Geoscience*, *3*(7), 468–472. doi: 10.1038/ngeo890

Kobarg. (1988). The tide-dependent dynamics of the Ekstroem Ice Shelf, Antarctica. *Berichte zur Polar- und Meeresforschung*, *50*.

Kristoffersen, Y., Hofstede, C., Diez, A., Blenkner, R., Lambrecht, A., Mayer, C., & Eisen, O. (2014). Reassembling Gondwana: A new high quality constraint from vibroseis exploration of the sub-ice shelf geology of the East Antarctic continental margin. *Journal of Geophysical Research: Solid Earth*, *119*(12), 9171–9182. doi: 10.1002/2014JB011479

Kuhn, G., & Gaedicke, C. (2015). A plan for interdisciplinary process.studies and geoscientific observations beneath the Eckstroem Ice Shelf (Sub-EIS-Obs). *Polarforschung*, *84*(2), 99–102.

Meijers, A. J. S., Meredith, M. P., Abrahamsen, E. P., Morales Maqueda, M. A., Jones, D. C., & Naveira Garabato, A. C. (2016). Wind-driven export of Weddell Sea slope water. *Journal of Geophysical Research: Oceans*, *121*(10), 7530–7546. doi: 10.1002/2016JC011757

Meredith, M. P., Gordon, A. L., Naveira Garabato, A. C., Abrahamsen, E. P., Huber, B. A., Jullion, L., & Venables, H. J. (2011). Synchronous intensification and warming of Antarctic Bottom Water outflow from the Weddell Gyre. *Geophysical Research Letters*, *38*(3), 1–4. doi: 10.1029/2010GL046265

Milillo, P., Rignot, E., Rizzoli, P., Scheuchl, B., Mouginot, J., Bueso-Bello, J., & Prats-Iraola, P. (2019). Heterogeneous retreat and ice melt of Thwaites Glacier, West Antarctica. *Science Advances*, *5*(1), 1–8. doi: 10.1126/sciadv.aau3433

Morlighem, M., Rignot, E., Binder, T., Blankenship, D., Drews, R., Eagles, G., . . . Young, D. A. (2020). Deep glacial troughs and stabilizing ridges unveiled beneath the margins of the Antarctic ice sheet. *Nature Geoscience*, *13*(2), 132–137. doi: 10.1038/s41561-019-0510-8

Neckel, N., Drews, R., Rack, W., & Steinhage, D. (2012). Basal melting at the Ekström Ice Shelf, Antarctica, estimated from mass flux divergence. *Annals of Glaciology*, *53*(60), 294–302. doi: 10.3189/2012AoG60A167

Nicholls, K. W., Abrahamsen, E. P., Buck, J. J. H., Dodd, P. A., Goldblatt, C., Griffiths, G., . . . Wilkinson, J. P. (2006). Measurements beneath an Antarctic ice shelf using an autonomous underwater vehicle. *Geophysical Research Letters*, *33*(8), L08612. doi: 10.1029/2006GL025998

Nøst, O. A. (2004). Measurements of ice thickness and seabed topography under the Fimbul Ice Shelf, Dronning Maud Land, Antarctica. *Journal of Geophysical Research*, *109*(11), 1–14. doi: 10.1029/2004JC002277

Nøst, O. A., Biuw, M., Tverberg, V., Lydersen, C., Hattermann, T., Zhou, Q., . . . Kovacs, K. M. (2011). Eddy overturning of the Antarctic Slope Front controls glacial melting in the Eastern Weddell Sea. *Journal of Geophysical Research*, *116*(11), 1–17. doi: 10.1029/2011JC006965

Padman, L., Erofeeva, S. Y., & Fricker, H. A. (2008). Improving Antarctic tide models by assimilation of ICESat laser altimetry over ice shelves. *Geophysical Research Letters*, *35*(22), L22504. doi: 10.1029/2008GL035592

Paolo, F. S., Fricker, H. A., & Padman, L. (2015). Volume loss from Antarctic ice shelves is accelerating. *Science*, *348*(6232), 327–331. doi: 10.1126/science.aaa0940

Patton, H., Swift, D., Clark, C., Livingstone, S., & Cook, S. (2016). Distribution and characteristics of overdeepenings beneath the Greenland and Antarctic ice sheets: Implications for overdeepening origin and evolution. *Quaternary Science Reviews*, *148*, 128–145. doi: 10.1016/j.quascirev.2016.07.012

Pattyn, F., Favier, L., Sun, S., & Durand, G. (2017). Progress in Numerical Modeling of Antarctic Ice-Sheet Dynamics. *Current Climate Change Reports*, *3*(3), 174–184. doi: 10.1007/s40641-017-0069-7

Pritchard, H. D., Ligtenberg, S. R., Fricker, H. A., Vaughan, D. G., Van Den Broeke, M. R., & Padman, L. (2012). Antarctic ice-sheet loss driven by basal melting of ice shelves. *Nature*, *484*(7395), 502–505. doi: 10.1038/nature10968

Rignot, E., Jacobs, S., Mouginot, J., & Scheuchl, B. (2013). Ice-Shelf Melting Around Antarctica. *Science*, *341*(6143), 266–270. doi: 10.1126/science.1235798

Ritz, C., Edwards, T. L., Durand, G., Payne, A. J., Peyaud, V., & Hindmarsh, R. C. (2015). Potential sea-level rise from Antarctic ice-sheet instability constrained by observations. *Nature*, *528*(7580), 115–118. doi: 10.1038/nature16147

Smetacek, V., Scharek, R., Gordon, L. I., Eicken, H., Fahrbach, E., Rohardt, G., & Moore, S. (1992). Early spring phytoplankton blooms in ice platelet layers of the southern Weddell Sea, Antarctica. *Deep Sea Research Part A, Oceanographic Research Papers*, *39*(2), 153–168. doi: 10.1016/0198-0149(92)90102-Y

Sun, S., Hattermann, T., Pattyn, F., Nicholls, K. W., Drews, R., & Berger, S. (2019). Topographic Shelf Waves Control Seasonal Melting Near Antarctic Ice Shelf Grounding Lines. *Geophysical Research Letters*, *46*(16), 9824–9832. doi: 10.1029/2019GL083881

Thompson, A. F., Stewart, A. L., Spence, P., & Heywood, K. J. (2018). The Antarctic Slope Current in a Changing Climate. *Reviews of Geophysics*, *56*(4), 741–770. doi: 10.1029/2018RG000624

Timmermann, R., & Hellmer, H. H. (2013). Southern Ocean warming and increased ice shelf basal melting in the twenty-first and twenty-second centuries based on coupled ice-ocean finite-element modelling. *Ocean Dynamics*, *63*(9-10), 1011–1026. doi: 10.1007/s10236-013-0642-0

Tinto, K. J., Padman, L., Siddoway, C. S., Springer, S. R., Fricker, H. A., Das, I., . . . Bell, R. E. (2019). Ross Ice Shelf response to climate driven by the tectonic imprint on seafloor bathymetry. *Nature Geoscience*, *12*(6), 441–449. doi: 10.1038/s41561-019-0370-2

Zhou, Q., Hattermann, T., Nøst, O. A., Biuw, M., Kovacs, K. M., & Lydersen, C. (2014). Wind-driven spreading of fresh surface water beneath ice shelves in the Eastern Weddell Sea. *Journal of Geophysical Research: Oceans*, *119*(6), 3818–3833. doi: 10.1002/2013JC009556

Supporting Information: Detailed seismic bathymetry beneath Ekström Ice Shelf, Antarctica: Implications for glacial history and ice-ocean interaction

Emma C. Smith[1], Tore Hattermann[2], Gerhard Kuhn[1], Christoph Gaedicke[3], Sophie Berger[1], Reinhard Drews[4], Todd A. Ehlers[4], Dieter Franke[3], Raphael Gromig[1] *, Coen Hofstede[1], Astrid Lambrecht[5], Andreas Läufer[3], Christoph Mayer[5], Ralf Tiedemann[1,6], Frank Wilhelms[1,7], Olaf Eisen[1,6]

[1]Alfred-Wegener-Institut Helmholtz-Zentrum für Polar- und Meeresforschung, Bremerhaven, Germany

[2]Norwegian Polar Institute, Tromsø, Norway

[3]BGR, Federal Institute for Geosciences and Natural Resources, Geozentrum Hannover, Hannover, Germany

[4]Department of Geosciences, University of Tübingen, Tübingen, Germany

[5]Geodesy and Glaciology, Bavarian Academy of Sciences and Humanities, Munich, Germany

[6]Department of Geosciences, University of Bremen, Bremen, Germany

[7]Department of Geosciences, University of Göttingen, Göttingen, Germany

*Now at: University of Cologne, Institute of Geology and Mineralogy, Cologne, Germany

Contents of this file

1. Text S1 to S4

Introduction This supporting information contains the following information about methods used in this study. The information is not crucial to the understanding of the main text, but will be of interest to some readers and those who may want to perform similar analysis.

- S1 - details of seismic data processing
- S2 - seismic velocity determination for depth conversion
- S3 - uncertainty calculations for the seismic bathymetry
- S4 - CTD data processing

S1: Seismic Data Processing

The following is a full description of the seismic vibroseis data processing steps, this process was followed for each seismic line in the survey:

1. Raw seismic vibroseis data were read from SEG2 field records into the Paradigm *EPOS* processing system.

2. Data were cross-correlated with the appropriate input vibroseis sweep to produce shot gathers.

3. Geometry was applied to locate the source and receiver positions and calculate common midpoint (CMP) positions.

4. Data were manually checked and compared to field logs to identify low quality shots and noisy or dead channels, which were then removed from further processing.

5. The data was bandpass filtered (survey dependent) and a notch filter at 206 Hz was applied, to remove known spurious noise from the geophones.

6. Data are then re-sorted into common midpoint (CMP) gathers.

7. CMP gathers with fold > 3 are used for velocity analysis, to determine the seismic-wave velocity (V_{stack}) of different layers within the sub-surface. This is done by fitting a normal moveout (NMO) velocity curve to the CMP gathers and in some areas using constant velocity stacks.

8. The velocity field produce by the above analysis is used for NMO correction of CMP gathers.

9. NMO corrected CMP gathers are stacked to produce one stacked trace for each CMP location, improving signal-to-noise ratio.

10. This stacked traces for each CMP location make up a time-stacked seismic section (example in main manuscript Fig. 2). It is the two-way traveltime of the reflection horizons on a time-stacked seismic section that are used to create the bathymetry map of the sea floor.

S2: Determination of Seismic Velocities for Depth Conversion

The seismic velocity used for depth conversion of the ice was derived from the average stacking velocity V_{stack}, determined during velocity analysis (Supporting Information S1). The value of V_{stack} can be assumed equal to the interval velocity (V_{int}) for ice, as it is a quasi-homogenous layer, and the reflection is from a near-horizontal surface (base of the ice shelf). The determined values of V_{stack} ranged from 3597 ms^{-1} to 3606 ms^{-1}, with an average value of 3601 ms^{-1}.

The depth-averaged seismic velocity value for the water column was determined using CTD profiles (main manuscript, Section 2.4) taken through the hot-water drilled access holes (main manuscript, Fig. 1c, blue circles). The TEOS-10 Matlab toolbox (McDougall & Barker, 2011) was used to make this calculation. The TEOS-10 toolbox implements the International Thermodynamic Equations Of Seawater - 2010 (IOC et al., 2010). The resulting seismic velocity values ranged from 1448 ms^{-1} to 1453 ms^{-1}, with an average of 1451 ms^{-1}. This value is comparable to values determined from CTD data under other Antarctic ice shelves (Brisbourne et al., 2014; Nøst, 2004; Rosier et al., 2018).

S3: Error Calculations for Seismic Derived Sea-floor Depths

Uncertainties in the sea-floor depth come from four sources, these will be analysed below: (1) accuracy of the horizon picking, (2) velocities used for depth conversion of these horizons, (3) errors in the REMA DEM used for surface elevation corrections and (4) depth errors from unmigrated data.

1. The error in horizon picking can be quantified by assessing the possible travel time mis-pick and converting this into a depth error. In the area of the main grid, the 2017 and 2018 surveys are high fold and the horizons are clear meaning picking of the peak of a reflection is possible to better than ± 1.5 ms. In the 2010 and 2011 surveys, the lower frequency Failing Y-1100 vibroseis source was used, which has a longer wavelength and lower resolution, such that picks are possible to ± 3 ms. However, with the exception of the far north eastern protrusion from the main seismic grid, picks from the 2017 and 2018 surveys were used preferentially in the gridding, therefore a picking error corresponding to ± 1.5 ms is appropriate for this region, giving a depth error of ± 7.6 m for the sea floor. The 2014 survey data is single fold, this doesn't affect the pick of the ice base, which is still possible to ± 1.5 ms, as it is largely horizontal. However, picks of the sea floor, in areas of rough topography are only possible to ± 15 ms, in the extreme case. This corresponds to a possible depth error of ± 27.2 m at the sea floor in the areas covered by these lines. As a result, the bathymetry map is significantly more accurate in the area of the main grid than the single lines that extend south across the grounding line.

2. The error in seismic velocity of the ice can be quantified by looking at the minimum and maximum velocities determined during velocity analysis (see S1). This yields a range

of ice velocities from 3597 ms^{-1} to 3606 ms^{-1}. The range of water column velocities determined from CTD measurements was 1448 ms^{-1} to 1453 ms^{-1}, giving a depth error at the deepest part of the sea floor from velocity errors of $\pm$ 4 m.

3. Seismic energy reflected from the sea floor is assumed to have reflected at the mid-point of the source and received, known as the CMP (see S1). However, for dipping interfaces this is not strictly true introducing an error, which is greatest for the deepest and steepest dipping interfaces. Using the dip-correction equations of (Yilmaz, 1987), an error of $\pm$ 2.4 m was calculated for the steepest dipping and deepest section of the sea floor.

4. The quoted error for the REMA DEM is $\pm$ 0.75 m in this region.

Summing these four error sources leads to a cumulative error at the sea floor of $\pm$ 14.8 m under the main data grid (at the ice shelf front) and $\pm$ 34.4 in the areas of the 2014 seismic lines, these values are stated in the main article.

S4: CTD Data Processing

CTD data were processed using the RBR Ruskin software, which was used to export pressure, in-situ temperature, and practical salinity data based on the sensor calibration that was obtained in October 2018 before the field season. The CTD profiles were split into individual down casts and up casts at each location and all data were inspected manually. Profiles showing obvious sensor drift and noise, which are often related to temporary accretion of ice crystals inside the conductivity cell in these environments, were discarded. The remaining data showed plausible water mass properties and structures beneath the ice shelf. Pre-season calibration data of the sensors was collected by the manufacturer, however, post-season calibration data were not available. Based on comparison of the data with established water mass properties in the region, uncertainties are assumed for in situ temperature (0.02°C) and salinity (0.03), yielding an accuracy that is similar to other datasets where post-calibration is not available (e.g. Treasure et al., 2017).

References

Brisbourne, A. M., Smith, A. M., King, E. C., Nicholls, K. W., Holland, P. R., & Makinson, K. (2014). Seabed topography beneath Larsen C Ice Shelf from seismic soundings. *The Cryosphere*, *8*(1), 1–13. doi: 10.5194/tc-8-1-2014

IOC, SCOR, & IAPSO. (2010). *The International Thermodynamic Equation of Seawater2010: Calculation and Use of Thermodynamic Properties, Intergovernmental Oceanographic Commission, Manuals and Guides No. 56.* University of Southampton: UNESCO.

McDougall, T. J., & Barker, P. M. (2011). *Getting started with TEOS-10 and the Gibbs*

Seawater (GSW) Oceanographic Toolbox,. SCOR/IAPSO WG127.

Nøst, O. A. (2004). Measurements of ice thickness and seabed topography under the Fimbul Ice Shelf, Dronning Maud Land, Antarctica. *Journal of Geophysical Research*, *109*(11), 1–14. doi: 10.1029/2004JC002277

Rosier, S. H. R., Hofstede, C., Brisbourne, A. M., Hattermann, T., Nicholls, K. W., Davis, P. E. D., ... Corr, H. F. J. (2018). A New Bathymetry for the Southeastern FilchnerRonne Ice Shelf: Implications for Modern Oceanographic Processes and Glacial History. *Journal of Geophysical Research: Oceans*, *123*(7), 4610–4623. doi: 10.1029/2018JC013982

Treasure, A., Roquet, F., Ansorge, I., Bester, M., Boehme, L., Bornemann, H., ... de Bruyn, P. N. (2017). Marine Mammals Exploring the Oceans Pole to Pole: A Review of the MEOP Consortium. *Oceanography*, *30*(2), 132–138. doi: 10.5670/oceanog.2017.234

Yilmaz, O. (1987). Chapter 4: Migration. In S. E. Doherty (Ed.), *Seismic data analysis: Processing, inversion, and interpretation of seismic data (i)* (pp. 463–653). Society of Exploration Geophysicists.